

Nonselective Wet Oxidation of AlGaAs Heterostructure Waveguides Through Controlled Addition of Oxygen

Yong Luo and Douglas C. Hall, *Member, IEEE*

Abstract—We present data showing that the addition of trace amounts of O_2 ($<1\%$ relative to N_2) to N_2+H_2O process gas during the wet thermal oxidation of $Al_xGa_{1-x}As$ enhances the oxidation rates of lower Al content ($x \leq 0.8$) alloys (a tenfold increase for $x = 0.3$), while decreasing the oxidation rate selectivity $R(x = 0.8)/R(x = 0.3)$ by a factor of seven. An increase in the refractive index from 1.49 to 1.68, and a fourfold decrease in surface roughness, indicates the formation of a denser, higher quality oxide for $x = 0.3$ AlGaAs. Oxides are characterized by prism coupling, atomic force microscopy, and scanning electron microscopy. Thermochemical calculations show a probable mechanism in the enhancement of the dry oxidation reactions of AlGaAs for low levels of O_2 , while there is still an adequate quantity of H_2 produced to reduce As oxides in the wet oxidation process. An AlGaAs quantum well heterostructure p-n laser diode crystal is nonselectively oxidized to create a deep oxide, high-index contrast waveguide with potential applications in semiconductor photonic integrated circuits that require small bend radius, high isolation, low crosstalk optical waveguides.

Index Terms—Integrated optoelectronics, materials processing, semiconductor films, semiconductor waveguides.

I. INTRODUCTION

THE 1990 discovery of the wet-thermal native oxides of AlGaAs [1] has led to significant advances within the field of optoelectronics. The much higher oxidation rate of AlAs relative to GaAs has enabled the selective oxidization of buried $Al_xGa_{1-x}As$ ($x \geq 0.85$) layers sandwiched between lower Al content AlGaAs or GaAs cladding layers [2]–[4]. The embedded oxide layer grown laterally inward from the exposed heterostructure edges of an etched mesa produces a useful current aperture, now widely employed in vertical-cavity surface-emitting lasers (VCSELs) with dramatic performance improvements [4]–[6] and excellent reliability; see, e.g., [7].

In AlGaAs and several other III–V alloy systems (e.g., AlInGaP, AlInAs, and AlGaSb), these native oxides provide a low refractive index ($n \sim 1.6$), insulating material useful in a variety of applications for both current and optical confinement [6], and offer strong potential for advanced photonic integration. However, in contrast to the ideal nature of selective lateral oxidation for the fabrication of VCSELs, the dramatic rate selectivity versus Al content in III–V alloys [6], [8]–[10] poses

processing limitations for edge-emitting geometries. Here, oxidation is generally restricted to high Al content ($x \geq 0.8$) upper cladding layers, whereas lower Al content layers are preferable for reliability reasons. Also, in fabricating oxide-confined index-guided edge-emitting lasers in an AlGaAs–GaAs quantum well heterostructure (QWH) [11], [12], the oxidation front cannot penetrate downward through the lower Al content waveguide region before the complete lateral oxidation of the higher Al content upper cladding layer (inward, under the contact stripe mask) pinches off the current path to the active region. Oxidizing only the upper cladding layer limits the maximum lateral effective index contrast for waveguides to $\Delta n \sim 0.05$ – 0.1 [13], limiting the minimum radius of curvature for bent waveguide structures [14]–[16]. One demonstrated solution for achieving “deep oxidation” through the active region for high index contrast waveguiding is a two-step process, in which Si impurity-induced layer disordering (IILD) [17] is first used to intermix the QWH, increasing the average Al content in the disordered waveguide for subsequent, enhanced oxidation [18]–[20].

In this work, we demonstrate the utility of controlled oxygen addition during wet oxidation to both greatly enhance the oxidation rate of low Al content $Al_xGa_{1-x}As$ ($x \leq 0.6$), while also reducing the rate selectivity to Al content, thereby providing, in effect, a simple and essentially “nonselective” oxidation technique. The detailed dependencies of oxidation rates of $Al_xGa_{1-x}As$ ($x = 0.3$ and 0.8), oxide refractive index, and surface roughness upon O_2 content in the water vapor carrier gas are studied, with a significant, favorable process modification obtained ($x = 0.3$) with only trace amounts ($<1\%$) of added O_2 (Section III). Here, we also demonstrate the deep oxidation of an AlGaAs QWH laser crystal without the need for IILD for applications requiring high index contrast waveguides (Section IV-A). This “mixed carrier gas” technique has also previously been employed to realize a substantial loss reduction in fully-oxidized AlGaAs single heterostructure planar waveguides [21], [22], potentially applicable in photonic integrated circuits for broadly transparent passive sections (Section IV-B). Finally, thermochemical calculations are presented to help illuminate the role of additional O_2 in modifying the wet thermal oxidation process chemistry for AlGaAs (Section V).

II. THE WET OXIDATION CARRIER GAS

A. Background: Known Effects of Oxygen

It has been shown that using pure O_2 as the carrier gas bubbled through H_2O completely suppresses the lateral oxidation

Manuscript received April 17, 2005. This work was supported by the National Science Foundation under Grant ECS-9502705 and Grant ECS-0123501.

Y. Luo was with the University of Notre Dame, Notre Dame, IN 46556 USA.

D. C. Hall is with the University of Notre Dame, Notre Dame, IN 46556 USA. (e-mail: dhall@nd.edu).

Digital Object Identifier 10.1109/JSTQE.2005.859024

of $\text{Al}_{0.98}\text{Ga}_{0.02}\text{As}$ [6]. While this result may lead to the belief that any added O_2 will suppress oxidation rates of any composition AlGaAs, earlier reports have shown that the addition of 0.1% (1000 parts per million, or ppm) O_2 to a N_2 carrier gas significantly reduces the reaction-rate activation energy and enhances oxidation rates for $\text{Al}_{0.6}\text{Ga}_{0.4}\text{As}$, while having very little effect on $\text{Al}_{0.77}\text{Ga}_{0.23}\text{As}$ [9]. In a previous study of the $\text{Al}_x\text{Ga}_{1-x}\text{As}$ native oxide refractive index for varied Al composition x (0.3–0.98) and oxidation temperatures, we observed a much higher refractive index for $x = 0.3$ –0.5 $\text{Al}_x\text{Ga}_{1-x}\text{As}$ oxides when oxidized with a small, unknown amount of O_2 contamination in the N_2 carrier gas from a malfunctioning ultrahigh purity (UHP) N_2 generator [21]. In this work, we report further investigations into this effect, in which we have controllably introduced O_2 to the $\text{N}_2 + \text{H}_2\text{O}$ process gas during oxidation of $\text{Al}_x\text{Ga}_{1-x}\text{As}$ ($x = 0.3$ and 0.8) to study the dependencies of oxidation rate, refractive index, and surface roughness on O_2 content.

B. Experimental Technique

The $\text{Al}_x\text{Ga}_{1-x}\text{As}$ heterostructures employed in this work are grown by metal organic chemical vapor deposition (MOCVD) at a growth temperature of 750°C . All layers are unintentionally doped. AlGaAs films oxidized in Section III studies have a thickness of $\sim 1\ \mu\text{m}$. After removal of a GaAs cap layer by wet chemical etching, the AlGaAs layers are oxidized at elevated temperatures (400 – 500°C) in water vapor carried into the 2-in tube furnace by bubbling N_2 through H_2O at 95°C . Maintaining our N_2 flow bubbled through the heated water at the 0.66 L/min, equivalent to the 1.4 scfh (sft³/hr) flow rate used in the original wet oxidation experiments [1] and in our previous studies [21], we now use an additional mass flow controller (calibrated with 5 sccm (cm³/min) full scale) to precisely mix UHP O_2 into the $\text{N}_2 + \text{H}_2\text{O}$ process gas after the bubbler, allowing O_2/N_2 ratios up to 0.005/0.66 or 0.76% (7600 ppm). The effects of higher O_2 concentrations are investigated by using premixed custom gases (with 1, 2, or 5% O_2 in N_2) passed as a mixed carrier gas through the water bubbler. We use the terminology “mixed carrier gas” whether the O_2 is mixed into the process gas stream before or after the H_2O bubbler, and despite the fact that the $\text{N}_2 + \text{O}_2$ gas is not a carrier gas in the conventional sense of being “inert,” as it clearly directly participates in the oxidation reactions. The actual concentration of O_2 relative to the total $\text{O}_2 + \text{N}_2 + \text{H}_2\text{O}$ process gas would be more difficult to determine or regulate, as the H_2O flow rate is a function of the H_2O vapor pressure in the heated bubbler and N_2 carrier gas flow rate.

III. OXYGEN ADDITION TO CARRIER GAS: EXPERIMENTAL RESULTS

A. The Effects of O_2 Addition on the Oxidation Rate of AlGaAs

Prism coupling measurements of the refractive index and thickness of the AlGaAs wet thermal native oxide films are performed with a Metricon Model 2010 instrument [21]. Oxidation times are varied to compensate for changing oxidation

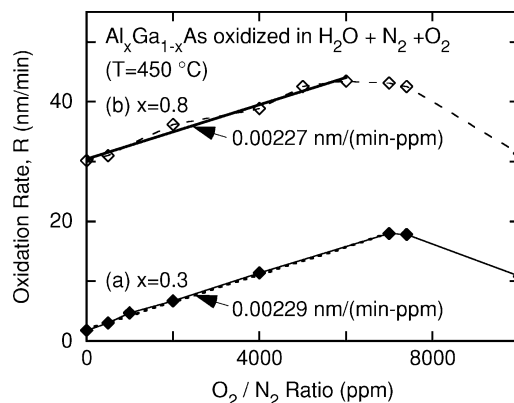


Fig. 1. Oxidation rates of (a) $\text{Al}_{0.3}\text{Ga}_{0.7}\text{As}$ and (b) $\text{Al}_{0.8}\text{Ga}_{0.2}\text{As}$ native oxides formed by mixing O_2 with the ultrahigh purity $\text{N}_2 + \text{H}_2\text{O}$ process gas.

rates to obtain films, where possible (up to ~ 7000 ppm O_2), with a thickness of ~ 0.8 – $0.9\ \mu\text{m}$ while avoiding overoxidation into the GaAs substrate. This ensures three optical modes in a nominally homogeneous single film for optimal prism coupler characterization. The index accuracy is ± 0.0001 , and the error of the thickness measurement is typically less than 0.3%. These accurate thickness measurements are used to determine the oxidation rates reported as follows, assuming linear growth rate dynamics [9], [10], [21].

Fig. 1 shows the effects of controlled O_2 addition to the process gas on the 450°C oxidation rates of (a) $\text{Al}_{0.3}\text{Ga}_{0.7}\text{As}$ [Fig. 1(a)] and (b) $\text{Al}_{0.8}\text{Ga}_{0.2}\text{As}$ [Fig. 1(b)]. The increasing oxidation rates satisfy a linear relationship for O_2 concentrations less than ~ 7000 ppm, as given by (1) and (2):

$$R = 2.09 + 0.00229C(\text{nm}/\text{min}), \quad (x = 0.3) \quad (1)$$

with a least squares fit correlation coefficient $r = 0.999$ for O_2 concentrations $C \leq 7000$ (ppm), and

$$R = 30.5 + 0.00227C(\text{nm}/\text{min}), \quad (x = 0.8) \quad (2)$$

with a fit correlation coefficient $r = 0.991$ for O_2 concentrations $C \leq 6000$ (ppm). In Fig. 1(a), for the lower Al composition $\text{Al}_{0.3}\text{Ga}_{0.7}\text{As}$, the oxidation rate (1) is dramatically increased by almost one order of magnitude for an O_2 concentration of 7000 ppm. In Fig. 1(b), for $\text{Al}_{0.8}\text{Ga}_{0.2}\text{As}$, the oxidation rate (2) is also increased at the same rate, but because the oxidation rate in UHP N_2 ($C = 0$) is much higher, the relative change is less significant. It is thus clear that the oxidation rate *selectivity* between high and low Al composition AlGaAs, drops dramatically for a properly selected ratio of O_2 to N_2 in the wet thermal oxidation process. For example, the rate selectivity $R(x = 0.8)/R(x = 0.3)$ at 450°C decreases from $(30.2\ \text{nm}/\text{min}) / (1.77\ \text{nm}/\text{min}) = 17.1\text{X}$ in UHP N_2 to $(43.2/17.9) = 2.4\text{X}$ with the addition of 7000 ppm O_2 relative to N_2 . At higher O_2 concentrations (>6000 – 7000 ppm), where the oxidation rate begins to drop, the oxide growth may become diffusion-limited by the formation of a denser oxide, such that the plotted rates, determined from a linear growth assumption, may no longer be strictly accurate. The behavior observed here

is explained in Section V with the aid of thermochemical calculations for the wet and dry oxidation reactions involved.

We note that the slopes of the changing rates versus O_2 concentration are very close: 0.00227 nm/(min-ppm) for $x = 0.3$ versus 0.00229 nm/(min-ppm) for $x = 0.8$. This suggests that O_2 addition similarly influences specific reactions in the oxidation of $Al_xGa_{1-x}As$, independent of Al composition, x . Other data (not shown) indicates that the slope of the oxygen-induced rate enhancement (the coefficient to C in (1) and (2)) is temperature dependent. For example, for $Al_{0.4}Ga_{0.6}As$ oxidized at 475 °C, the slope is increased to 0.00323 nm/(min-ppm), and for $Al_{0.3}Ga_{0.7}As$ oxidized at 500 °C, the slope is further increased to 0.00398 nm/(min-ppm).

We have looked for a rate enhancement with O_2 added during the lateral oxidation of a 50 nm $Al_{0.98}Ga_{0.02}As$ layer of the type widely employed in VCSEL structures, although in such applications the decrease in rate selectivity to Al content would generally be undesirable. No rate enhancement is detectable at 430 °C with 7000 ppm O_2 . The expected enhancement of ~ 10 nm/min at this O_2 content and temperature (extrapolated from enhancement slopes at 450–500 °C given previously) is simply immeasurable and negligible relative to the 1.17 $\mu\text{m}/\text{min}$ rate observed with 0 ppm O_2 .

While the use of O_2 addition during wet oxidation may not be beneficial for VCSEL structures, it is significant for its ability to extend the use of wet thermal oxidation technology to—and potentially enable new optoelectronics applications in—AlGaAs heterolayers with lower Al content. While wet thermal oxidation of an upper $Al_{0.6}Ga_{0.4}As$ cladding layer was used in [12] to form high performance index-guided lasers, the slow oxidation rate required utilization of a thinner ($\sim 0.5 \mu\text{m}$) cladding layer than is typically employed, and an undesirably high oxidation temperature of 525 °C. With the enhanced oxidation rates achieved through the controlled addition of O_2 , not only can oxidation temperatures be reduced to more reasonable values, but the reduced selectivity to Al composition makes it possible to oxidize deeply into, or through, AlGaAs heterostructures containing low Al composition ($x \leq 0.6$) layers, as are typically used in semiconductor laser heterostructures, without the problems otherwise encountered as mentioned in Section I. Two applications for this nonselective oxidation of AlGaAs heterostructure waveguides are discussed in Section IV.

B. The Effects of O_2 Addition on the AlGaAs Oxide Quality: Refractive Index and Surface Roughness

The dependencies of refractive index on the concentration of O_2 relative to the N_2 in the carrier gas are shown in Fig. 2(a) for $Al_{0.3}Ga_{0.7}As$ and Fig. 2(b) for $Al_{0.8}Ga_{0.2}As$ wet oxidized at 450 °C. For the oxide of $Al_{0.3}Ga_{0.7}As$, the index increases from 1.49 to 1.65 with just 500 ppm O_2 present, and remains near 1.68, with only slight variations, for O_2 concentrations up to 1%. Such increases in index were observed and reported in [21], though the exact O_2 concentration in the carrier gas was unknown. Fig. 1 shows that for $Al_{0.8}Ga_{0.2}As$ oxidized with less than 8000 ppm O_2 present, the oxide index remains relatively constant at around 1.56. With more than 8000 ppm O_2 , the oxide

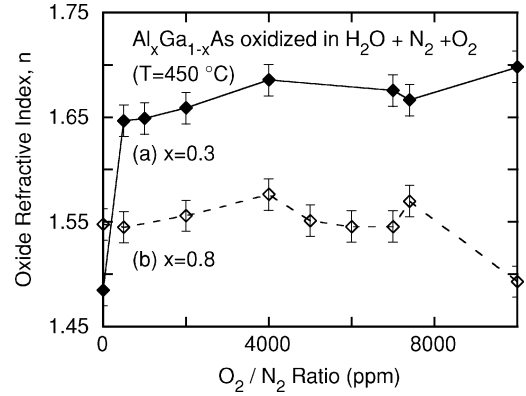


Fig. 2. Refractive indices of (a) $Al_{0.3}Ga_{0.7}As$ and (b) $Al_{0.8}Ga_{0.2}As$ native oxides formed by mixing O_2 with the ultrahigh purity $N_2 + H_2O$ process gas.

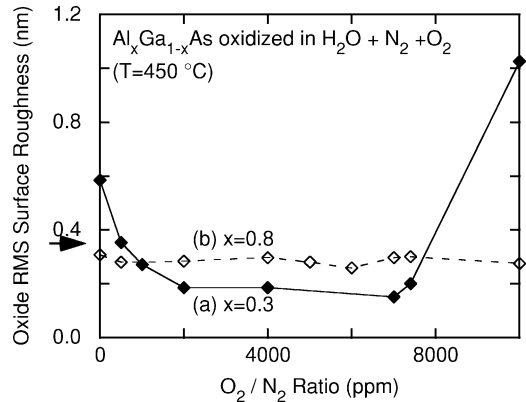


Fig. 3. Surface roughness dependencies on the O_2 concentration for (a) $Al_{0.3}Ga_{0.7}As$, and (b) $Al_{0.8}Ga_{0.2}As$ native oxides. The arrow on the Y axis marks the rms value of the $Al_{0.3}Ga_{0.7}As$ semiconductor surface roughness after etching away the cap layer.

index comes down to around 1.5. The effects of O_2 addition on oxide index are clearly stronger for low Al composition $Al_xGa_{1-x}As$. As the refractive index is an indirect measure of the film density, the higher observed index indicates formation of a denser, less porous oxide of low Al content AlGaAs, possibly closer in stoichiometry to $(Al_xGa_{1-x})_2O_3$, and which could reasonably be expected to have better insulating properties.

It has been reported that using air ($\sim 20\%$ O_2) as the water vapor carrier gas during wet thermal oxidation of AlGaAs results in very rough oxide films [9]. Measurements using a Digital Instruments atomic force microscope (AFM) on the samples shown in Figs. 1 and 2 were done to study how the oxide surface roughness depends on O_2 concentration, and to demonstrate the higher quality of the wet thermal oxides grown here using much more dilute O_2 concentrations. Fig. 3 shows the surface roughness dependencies of $Al_{0.3}Ga_{0.7}As$ [Fig. 3(a)] and $Al_{0.8}Ga_{0.2}As$ [Fig. 3(b)] native oxides on O_2 concentration. The arrow on the Y-axis marks the rms value of 0.35 nm for the $Al_{0.3}Ga_{0.7}As$ semiconductor surface immediately after etching away the GaAs cap layer with a selective citric peroxide etch (4:1 citric acid: H_2O_2) and before oxidation. Unexpectedly, for $Al_{0.3}Ga_{0.7}As$ native oxides, the rms

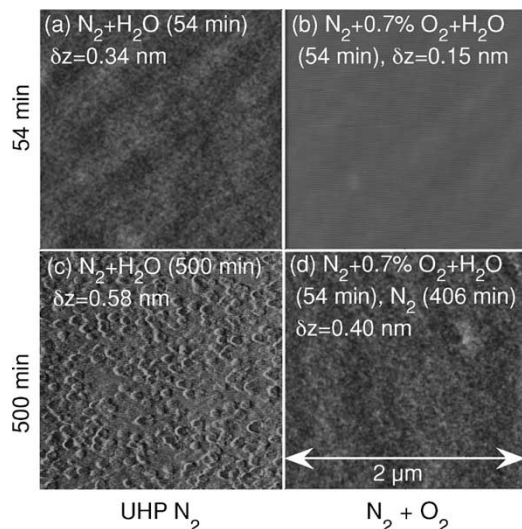


Fig. 4. Atomic force microscopy (AFM) image matrix showing the surface roughness of four $\text{Al}_{0.3}\text{Ga}_{0.7}\text{As}$ oxide samples with different wet oxidation conditions as follows: (a) oxidized at 450°C for 54 min with UHP $\text{N}_2+\text{H}_2\text{O}$; (b) oxidized at the same temperature for 54 min with 0.7% O_2 present in UHP $\text{N}_2+\text{H}_2\text{O}$; (c) oxidized at 450°C for 500 min with UHP $\text{N}_2+\text{H}_2\text{O}$; and (d) oxidized at 450°C for 54 min with $\text{N}_2 + 0.7\%\text{O}_2+\text{H}_2\text{O}$ and then held at 450°C another 406 min in UHP N_2 only. Each image represents a $2\text{-}\mu\text{m}$ -square scan field.

roughness decreases from 0.59–0.15 nm while the O_2 concentration increases to 7000 ppm. The rms roughness then increases to 1.03 nm at 10000 ppm. The improvement in surface quality of $\text{Al}_{0.8}\text{Ga}_{0.2}\text{As}$ oxides is not observed, and the rms roughness remains around 0.29 nm.

The smoother surfaces of $\text{Al}_{0.3}\text{Ga}_{0.7}\text{As}$ native oxides formed with O_2 added to the process gas are attributed to a shorter oxidation time, denser oxide, and possibly different products in the oxide film. An AFM image “matrix” of four $\text{Al}_{0.3}\text{Ga}_{0.7}\text{As}$ oxide films is shown in Fig. 4 to compare the relative effects of process time versus O_2 content on the surface quality. Sample (b) oxidizes in only 54 min with the addition of 0.7% O_2 (resulting in the smoothest surface, $\delta z = 0.15$ nm), while sample (c) is oxidized with a UHP N_2 water vapor carrier gas (i.e., without added O_2) for 500 min to achieve the same $\sim 0.9\ \mu\text{m}$ oxide thickness (resulting in the roughest surface, $\delta z = 0.58$ nm). The top two samples in Fig. 4 are both oxidized at 450°C for 54 min with sample (a) UHP N_2 and sample (b) with 0.7% O_2 relative to N_2 , such that the resulting oxide thickness in sample (a) is much less than that of sample (b). By comparing the rms roughness of sample (c) and (a) to sample (b), we see that reduced oxidization time cannot be the only factor leading to the much smoother surface of sample (a) relative to sample (c). Both sample (a) and (b) are oxidized for 54 min, but the roughness of (a) oxidized without added O_2 is more than twice that of (b). We believe that the greater density of the oxide grown with O_2 addition (as evidenced by a higher refractive index) contributes significantly to a reduction in the oxide surface roughness by “capping” and suppressing dissociation of the III–V crystal.

Samples (c) and (d) at the bottom in Fig. 4 were both “processed” for 500 min at 450°C . While the sample in Fig. 4(c) was wet oxidized at 450°C for 500 min with a UHP N_2 car-

rier gas, sample (d) was oxidized as in (b) for 54 min with $\text{N}_2 + 0.7\%\text{O}_2$ and then held at 450°C another 406 min in UHP N_2 . The $\delta z = 0.40$ nm roughness of sample (d) is much larger than that of the similarly oxidized but unannealed sample of (b), showing that at longer process times crystal dissociation does increase roughness. Although the total process times of samples (c) and (d) are the same and the oxide thicknesses comparable, sample (d) oxidized with 0.7% O_2 still has a smoother surface than that of sample (c). This further confirms that process time is not the only source of roughness reduction between $\sim 0.9\text{-}\mu\text{m}$ -oxide samples (c) and (b), but that with O_2 added, the formation of a denser oxide (with possibly different chemical or structural composition), and its more rapid formation (that quickly “seals” the sample more effectively against ongoing dissociation effects), together serve to reduce the surface roughness.

IV. NONSELECTIVE OXIDATION OF AlGaAs HETEROSTRUCTURE WAVEGUIDES

A. High Index Contrast Oxide Confined Waveguides

As described in Section I, a large lateral index contrast is desirable in two-dimensional waveguide structures for integrated optoelectronic devices such as semiconductor heterostructure lasers, and particularly to fabricate curved ring resonators or routing waveguides in photonic integrated circuits having low bend loss, good optical isolation, and low crosstalk between adjacent guides [19].

In the two-step process demonstrated by Krames *et al.* [18]–[20], Si impurity-induced layer disordering (IILD) [17] is employed before oxidation. The oxidation front can then penetrate downward through the IILD-intermixed (Al-composition averaged) waveguide region to form a “deep oxide” with an index of $n \sim 1.6$ that is much lower than that of the unoxidized $\text{Al}_x\text{Ga}_{1-x}\text{As}$ ($n \sim 3.5$, depending on x), resulting in a real lateral index contrast of $\Delta n \sim 1.7\text{--}1.9$. The lateral index step controlling waveguiding, however, might effectively be the lower index step ($\Delta n \sim 0.3\text{--}0.4$) that the guided wave first encounters at the Si diffusion interface where the heterostructure providing vertical waveguiding i.e., largely obliterated by heavy layer intermixing. “Deep-oxide” s-bend waveguides with $100\ \mu\text{m}$ offsets have exhibited low excess bend losses with a 3 dB transition distance less than $140\ \mu\text{m}$, significantly lower than those measured for oxide-only and disordered-only guides [19]. The IILD step adds complexity to the process by requiring an As overpressure and process temperatures of $\sim 850^\circ\text{C}$ for 7 h or longer [19]. The Si diffusion employed also introduces doping impurities, which may have undesirable implications for the device electrical performance and can cause increased optical free carrier absorption loss. We demonstrate here a new process for deep oxidation of an AlGaAs QWH laser crystal, without the need for IILD, achieved with only a simple modification of the wet thermal oxidation process gas by exploiting the O_2 enhancement effect shown in Section III-B, to provide a greatly reduced oxidation rate selectivity to Al composition. The approach is much simpler than the two-step combined IILD and oxidation process,

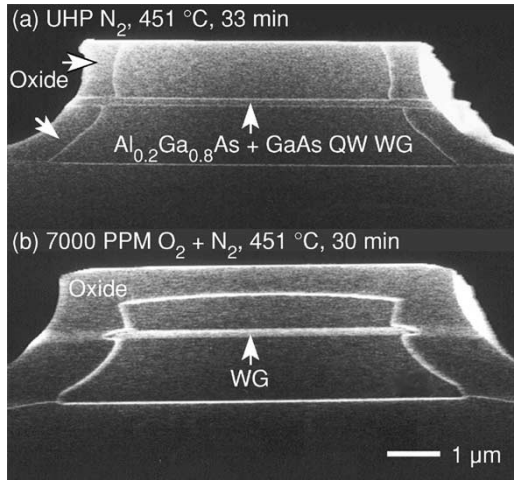


Fig. 5. Quantum well heterostructure (QWH) *p-n* laser diode crystal oxidized laterally (a) in UHP N_2 at 451 °C for 33 min, and (b) with mixed 7000 ppm $O_2 + N_2$ at 451 °C for 30 min. In (a), only the $Al_{0.8}Ga_{0.2}As$ cladding layers are oxidized, to a depth of $\sim 0.55 \mu m$, while the $Al_{0.2}Ga_{0.8}As$ waveguide layers with GaAs QW remain unoxidized. In (b), the oxidation rate selectivity with Al content is clearly reduced and both the GaAs cap and waveguide layers are oxidized in addition to the $Al_{0.8}Ga_{0.2}As$, with lateral oxidation depths ranging from 1.1–1.5 μm . No anisotropic oxide spike along the doped cladding/undoped waveguide interfaces, as seen in [37], is observed here.

and may provide a new means for realizing practical (i.e., easily manufacturable) and truly high-index-contrast waveguides for future photonic integrated circuits.

The application of this reduced rate selectivity to deep oxidation is explored using a conventional single quantum well heterostructure (QWH) *p-n* laser diode wafer custom grown via MOCVD by Epitaxial Products Inc. (now IQE Inc.). The structure consists of an undoped 10 nm GaAs QW sandwiched between two undoped 75 nm $Al_{0.2}Ga_{0.8}As$ epilayers forming the waveguide. The waveguide is surrounded by $\sim 1 \mu m$ thick $Al_{0.8}Ga_{0.2}As$ upper and lower current confining layers doped p-type (Zn, $N_A \sim 9.5 \times 10^{17} cm^{-3}$) and n-type (Si, $N_D \sim 1.8 \times 10^{18} cm^{-3}$), respectively. The n-type substrate and 500 nm GaAs buffer layer are doped with $1-4 \times 10^{18} cm^{-3}$ Si, and the 50 nm p-type GaAs cap is heavily doped with $>1 \times 10^{19} cm^{-3}$ Zn.

The effects of UHP $N_2 + H_2O$ and mixed $O_2 + N_2 + H_2O$ process gas on the oxidation of this QWH have been investigated for both etched ridge and buried (planar structure) 2-D waveguide geometries. After patterned by standard photolithographic techniques with photoresist, a stripe mesa is etched using non-selective sulfuric peroxide (1:8:80 $H_2SO_4:H_2O_2:H_2O$) to an arbitrary point below the lower confining layer. The isotropic wet etch results in lateral etching of up to 2 μm from both sides beneath the edges of the masked stripes. For the scanning electron microscope (SEM) cross sectional images shown in this section, the oxidized samples are first stained using 1:4:40 $HCl:H_2O_2:H_2O$ for ~ 15 s. The SEM cross sections in Fig. 5 show the ridge waveguide wet oxidized sample [Fig. 5(a)] using UHP N_2 carrier gas at 451 °C for 33 min, and [Fig. 5(b)] with mixed carrier gas of 7000 ppm O_2 relative to N_2 at 451 °C for 30 min. Ordinarily, the mesa would be protected with a Si_3N_4

cap layer to prevent oxidation of the contact region when fabricating a laser diode device, but in this experiment, the nitride layer is omitted on both samples shown in Fig. 5(a) and (b) in order to observe whether the GaAs cap layer alone can prevent oxidation through the surface. The difference is dramatic, as shown in Fig. 5(b), which demonstrates clearly that the mixed $O_2 + N_2$ carrier gas promotes a much stronger oxidation effect for both low Al-content AlGaAs ($x = 0.2$) and the p^+ GaAs cap. In Fig. 2(a), the GaAs cap layer protects the underlying $Al_{0.8}Ga_{0.2}As$ layer from oxidation, and the high rate selectivity to Al content results in 0.6 μm of lateral oxidation of the $Al_{0.8}Ga_{0.2}As$ confining layers while no lateral oxidation of the $Al_{0.2}Ga_{0.8}As$ waveguide plus GaAs QW region is evident. In marked contrast, Fig. 5(b) shows that with O_2 added to the process gas the GaAs cap layer cannot prevent oxidation from the surface, and that both the $Al_{0.8}Ga_{0.2}As$ confining layers and the $Al_{0.2}Ga_{0.8}As + GaAs$ QW waveguide are clearly laterally oxidized $\sim 1-1.25 \mu m$ with very little selectivity. For fabrication of devices, oxidation of the GaAs cap can be prevented by using a Si_3N_4 mask. After oxidation, the Si_3N_4 layer stripe mask can be removed via reactive ion etching in a CF_4 plasma, which does not attack the AlGaAs native oxide [22]. High-index contrast ring resonator lasers recently fabricated using this process have been reported elsewhere [23].

From the result shown in Fig. 5(a), it appears that useful etched mesa-geometry ridge waveguide lasers with strong lateral effective index contrast could also be realized from selective lateral oxidation of only the upper and lower cladding layers with a UHP N_2 carrier gas, similar to the undoped, top and bottom native oxide embedded photopumped laser of [2]. We note that previous attempts to realize deep oxidation in an etched ridge waveguide [as shown in Fig. 5(a)], or to achieve deep oxidation (i.e., through the waveguide layers and below the *p-n* transition) from a planar (non-etched) geometry on similar *p-n* doped QWH laser crystals, revealed an apparent photon-induced anodic oxidation reaction at the *p*-side waveguide/confining layer interface [24]. This phenomenon was observed to cause the formation of an anisotropic oxide “spike” protruding laterally to pinch off the current path [24]. From the SEM figures presented in Fig. 5, we see no evidence of a pronounced anodic oxidation reaction and anisotropic oxide spike formation at the boundary between the *p*-type $Al_{0.8}Ga_{0.2}As$ upper confining layer and the undoped waveguide. While the effect may be doping dependent, the doping of the QWH used in this work is typical of standard *p-n* junction diode structures. The discrepancy between the results observed here and previous reports [24] suggests that the anisotropic oxidation effect is a growth-related issue, and not a fundamental limitation for the formation of deep-oxide waveguides.

B. Fully-Oxidized AlGaAs Heterostructure Waveguides

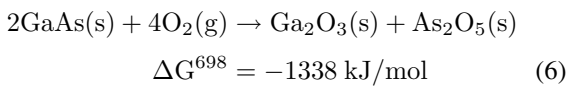
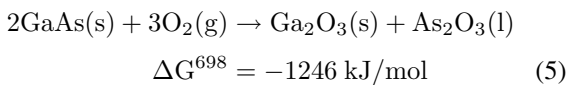
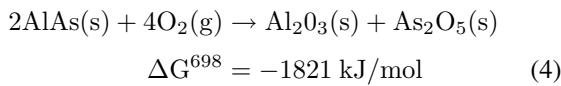
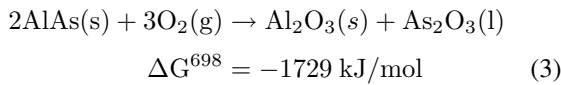
We have elsewhere demonstrated that with the large refractive index variation of wet-thermally oxidized $Al_xGa_{1-x}As$ with Al composition (x) [21], fully-oxidized AlGaAs heterostructures can support waveguiding within the oxide itself [25]. With the addition of O_2 during wet thermal oxidation, the higher

resulting refractive index contrast between oxides of different Al content AlGaAs (Section III-A) leads to better optical mode confinement, which in turns reduces absorption of higher photon energy light in the underlying GaAs substrate. When an O_2 concentration around 7000 ppm is used in the fabrication of an oxide heterostructure waveguide with a $1.5 \mu\text{m}$ lower cladding layer ($x = 0.85$), a $1.5 \mu\text{m}$ core layer ($x = 0.3$), and no top cladding layer, a substantial reduction in surface roughness for the lower Al content guiding layer material (Section III-B) leads to reduced interface scattering and a substantial reduction in the propagation loss is achieved. Compared to 10.9 dB/cm at $1.55 \mu\text{m}$ and $>30 \text{ dB/cm}$ (detection limit) at 633 and 830 nm in [25], loss is reduced to values of 4.0 dB/cm at $1.55 \mu\text{m}$, 3.6 dB/cm at $1.3 \mu\text{m}$, 4.3 dB/cm at 830 nm , and 5.0 dB/cm at 633 nm (data not shown) [26], [27]. In effect, we have demonstrated that an absorbing semiconductor waveguide can be converted to a wide bandgap ($E_g \sim 4\text{--}5 \text{ eV}$) oxide waveguide that is relatively transparent for photons of wavelengths well beyond the absorption edge of both GaAs or $\text{Al}_{0.3}\text{Ga}_{0.7}\text{As}$. These values compare favorably to the 8.5 dB/cm losses reported in passive bandgap-tuned AlGaAs/GaAs waveguides fabricated via quantum-well intermixing at the lasing wavelength of 860 nm of the as-grown material [28]. One potential application of fully oxidized AlGaAs heterostructure waveguides is a GaAs-based Er-doped native oxide waveguide amplifier in which pump and/or signal lasers could be monolithically integrated. We have elsewhere demonstrated the suitability of AlGaAs native oxides as a host for optically active Er^{3+} [29], [30].

V. OXYGEN ADDITION TO CARRIER GAS: THERMOCHEMICAL CALCULATIONS

The use of thermochemical calculations to illuminate the wet thermal oxidation process for AlAs was first presented by Ashby [31]. The role of added O_2 in wet thermal oxidation is elucidated here by considering the thermochemistry of the following dry and wet oxidation reactions of AlAs versus GaAs.

1 Dry oxidation reactions:



2 Wet oxidation reactions:

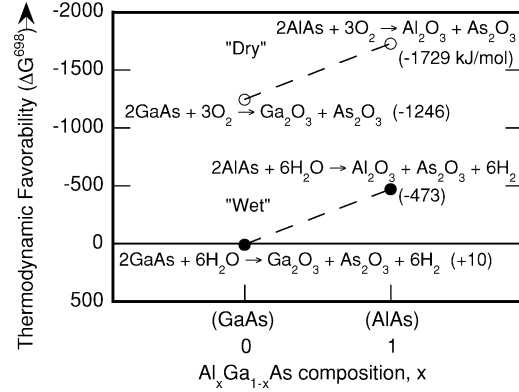
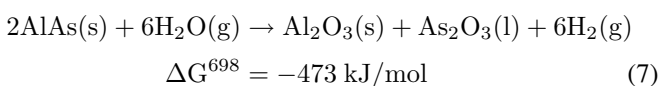


Fig. 6. Comparison of Gibbs free energy at $T = 698 \text{ K} = 425 \text{ }^\circ\text{C}$, ΔG^{698} , for wet and dry oxidation reactions for AlAs and GaAs. Thermodynamic favorability increases upward as ΔG^{698} becomes more negative.

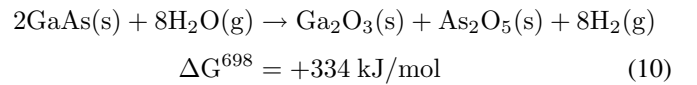
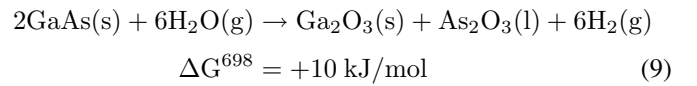
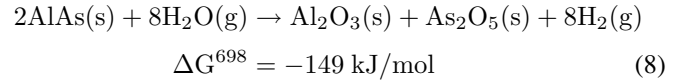
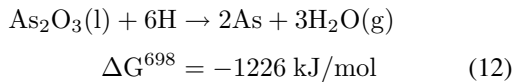
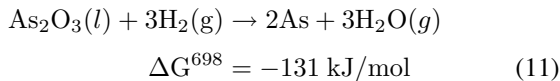


Fig. 6 plots the Gibbs free energies ΔG^{698} (the measurement of thermodynamic favorability of the reaction, which increases as ΔG^{698} becomes more negative) at the oxidation temperature of $T = 698 \text{ K}$ ($425 \text{ }^\circ\text{C}$) for dry oxidation reactions of AlAs (3) and GaAs (5) and the wet oxidation reactions of AlAs (7) and GaAs (9), calculated using the material data and procedures outlined in [32]. It is clear that the dry oxidation reactions produce more energy, and are thus more favorable than those of wet thermal oxidation. It is, then, not surprising that added O_2 increases oxidation rates by driving the more favorable dry reactions. The dashed lines in Fig. 6 are linear interpolations to guide the eye and suggest the approximate values expected for the AlGaAs ternary alloys. It can be seen that, in contrast to the thermodynamically unfavorable wet oxidation reactions of GaAs in (9) or (10), that the decrease in favorability as the Al content in an AlGaAs alloy is decreased is expected to be relatively less significant for the dry oxidation reactions, offering insight into why the oxidation rate selectivity between high and low Al content AlGaAs could be reduced with the introduction of O_2 , which enhances the dry O_2 reactions in conjunction with the wet thermal oxidation process.

The preceding thermochemical calculations of ΔG^{698} give only thermodynamic favorabilities of individual reactions. Clearly, other dynamics must be considered to understand why too much O_2 suppresses oxidation, and why GaAs and AlAs oxidize much more readily in wet ($\text{N}_2 + \text{H}_2\text{O}$) rather than dry (O_2 only) thermal oxidation environments. This other dynamic is the removal of As from the matrix. The important work by Ashby *et al.* [30] has shown that hydrogen liberated during wet thermal oxidations (7) is necessary for the dry oxidation product

As₂O₃ to be converted to the more volatile elemental As



These reactions allow the removal of As from the reacting layer, and reduce the thickness of the denser As₂O₃ oxide layer at the oxidation front that can block the diffusion of reactants and byproducts when too thick. Twستن *et al.* have shown with TEM studies that at the progressing oxidation front in laterally oxidized AlAs, there is a dense, amorphous region with a steady state thickness of ~17 nm [33], [34]. This region is believed to be rich in As oxide, the intermediate product, subsequently reduced as in (11) and (12), leaving behind a porous Al₂O₃ matrix through which oxidants and As readily diffuse.

In Ashby's work, only As₂O₃ was discussed as the arsenic oxide byproduct in wet-thermal oxidation reactions [24]. Because As₂O₅ has also been recently identified in oxidized Al_xGa_{1-x}As ($x = 0.96$) [35], we have included the reactions with this byproduct as well. Our thermochemical calculations for the wet oxidation of AlAs indicate that the formation of As₂O₅ is also thermodynamically favorable ($\Delta G^{698} = -149$ kJ/mol, (8)), though less so than that for As₂O₃ ($\Delta G^{698} = -473$ kJ/mol, (7)). However, for dry oxidation reactions (3)–(6), the reactions producing As₂O₅ from AlAs ($\Delta G^{698} = -1821$ kJ/mol, (4)) and GaAs ($\Delta G^{698} = -1338$ kJ/mol, (6)) are slightly more favorable than their As₂O₃ producing counterparts ($\Delta G^{698} = -1729$ kJ/mol, (3) and $\Delta G^{698} = -1246$ kJ/mol, (5), respectively). The wet thermal oxidation reactions of GaAs producing both As₂O₃ ($\Delta G^{698} = +10$ kJ/mol, (9)) and As₂O₅ ($\Delta G^{698} = +334$ kJ/mol, (10)) have positive Gibbs free energies and are, therefore, not thermodynamically favorable. However, these reactions can also occur to some degree through the absorption of heat released from other reactions or from the furnace.

Having discussed the important role of H in As removal [31], the declining oxidation rate with further increases in O₂ content beyond ~7000 ppm in Fig. 1 is easily understood. As more and more O₂ is added into the process gas, the stronger dry oxidation reaction begins displacing the wet oxidation reaction, such that more and more As₂O₃ and As₂O₅ at the oxidation front is produced without the accompanying production of H₂ (released only in the wet reaction) needed to reduce the As oxides to the more volatile As for removal from the crystal, (6), (7). While the As oxides are volatile at the oxidation temperatures, they are much larger molecules than As or As₂, and apparently not easily transported through the porous oxide microstructure. As the dense As₂O₃/As₂O₅ intermediate product region formed at the oxidation front becomes thicker, the diffusion of reactants and byproducts slows down, reducing the oxidation rate, and the oxidation kinetics may transition from linear (reaction rate limited) to parabolic (diffusion limited) behavior [36]. With a high enough O₂ concentration, the oxidation is eventually suppressed altogether, with a terminus formed [9]. At 2% O₂ concentration, we have observed that the thickness of oxidized

Al_{0.8}Ga_{0.2}As appears to saturate or terminate at a depth of about 350 nm, consistent with diffusion limited oxide growth. For Al_{0.3}Ga_{0.7}As, an oxide terminus appears to be formed with a very rough surface when the O₂ concentration is ≥5%. In the case of purely dry oxidation with O₂, the oxidation rate is much lower than that of wet oxidation with UHP N₂ or mixed carrier gas because of the complete absence of hydrogen necessary for the removal of As from the oxide film.

VI. CONCLUSION

We have presented data showing that the addition of trace amounts of O₂ (<1% relative to N₂) to the N₂+H₂O process gas during the wet thermal oxidation of Al_xGa_{1-x}As enhances the oxidation rate of lower Al content alloys ($x < 0.8$), decreases the oxidation rate selectivity to Al content and, for $x = 0.3$, increases the oxide refractive index and decreases its surface roughness. Thermochemical calculations of relevant oxidation reactions are presented to show that the enhancement of the dry oxidation reactions of AlGaAs is a probable mechanism responsible for the observed rate enhancement and selectivity modification. The resulting higher index contrast and reduced scattering achieved through O₂ addition enables a significant reduction in propagation loss in fully-oxidized AlGaAs heterostructure planar waveguides, with losses as low as 3.6 dB/cm at 1.3 μm, and 5.0 dB/cm above the GaAs bandgap at 633 nm, achieved. The capability for nonselective oxidation of Al-GaAs waveguide heterostructures realized by this simple process gas modification makes possible a new technique for the deep oxidation of a QWH laser diode crystal, eliminating the requirement for an additional impurity-induced layer disordering (IILD) step before oxidation. The process may offer a viable approach for the development of high-confinement, small bend radius, low-loss waveguides for semiconductor photonic integrated circuits.

ACKNOWLEDGMENT

The authors are grateful to H. Hou (now at EMCORE West), A. A. Allerman, and O. Blum of Sandia National Laboratory for providing some of the heterostructures used in this work.

REFERENCES

- [1] J. M. Dallesasse, N. Holonyak, Jr., A. R. Sugg, T. A. Richard, and N. El-Zein, "Hydrolyzation oxidation of Al_xGa_{1-x}As-AlAs-GaAs quantum well heterostructures and superlattices," *Appl. Phys. Lett.*, vol. 57, pp. 2844–2846, 1990.
- [2] A. R. Sugg, E. I. Chen, T. A. Richard, N. Holonyak, Jr., and K. C. Hsieh, "Native oxide-embedded Al_yGa_{1-y}As-GaAs-In_xGa_{1-x}As quantum-well heterostructure lasers," *Appl. Phys. Lett.*, vol. 62, pp. 1259–1261, 1993.
- [3] S. A. Maranowski, A. R. Sugg, E. I. Chen, and N. Holonyak, Jr., "Native oxide top- and bottom-confined narrow stripe p-n Al_yGa_{1-y}As-GaAs-In_xGa_{1-x}As quantum-well heterostructure laser," *Appl. Phys. Lett.*, vol. 63, pp. 1660–1662, 1993.
- [4] D. L. Huffaker, D. G. Deppe, K. Kumar, and T. J. Rogers, "Native-oxide defined ring contact for low threshold vertical-cavity lasers," *Appl. Phys. Lett.*, vol. 65, pp. 97–99, 1994.
- [5] K. D. Choquette, Jr., R. P. Schneider, K. L. Lear, and K. M. Geib, "Low threshold voltage vertical-cavity laser fabricated by selective oxidation," *Electron. Lett.*, vol. 30, no. 24, pp. 2043–2044, Nov. 1994.

- [6] K. D. Choquette, K. M. Geib, C. I. H. Ashby, R. D. Twesten, O. Blum, H. Q. Hou, D. M. Follstaedt, B. E. Hammons, D. Mathes, and R. Hull, "Advances in selective wet oxidation of AlGaAs alloys," *IEEE J. Sel. Topics. Quantum Electron.*, vol. 3, no. 3, pp. 916–926, Jun. 1997.
- [7] J. K. Guenter, J. A. Tatum, A. Clark, R. S. Penner, R. H. Johnson, R. A. Hawthorne, J. R. Biard, and Y. Liu, "Commercialization of honeywell's VCSEL technology: Further developments," *Vertical Cavity Surface Emitting Lasers V, Proc. SPIE-Int. Soc. Opt. Eng.*, K. D. Choquette and C. Lei, Eds., vol. 4286, 2001.
- [8] F. A. Kish, S. J. Caracci, N. Holonyak, Jr., K. C. Hsieh, J. E. Baker, S. A. Maranowski, A. R. Sugg, J. M. Dallesasse, and R. M. Fletcher, "Properties and use of $\text{In}_{0.5}(\text{Al}_x\text{Ga}_{1-x})_{0.5}\text{P}$ and $\text{Al}_x\text{Ga}_{1-x}\text{As}$ native oxides in heterostructure lasers," *J. Electron. Mater.*, vol. 21, pp. 1133–1139, 1992.
- [9] R. S. Burton and T. E. Schlesinger, "Wet thermal oxidation of $\text{Al}_x\text{Ga}_{1-x}\text{As}$ compounds," *J. Appl. Phys.*, vol. 76, pp. 5503–5507, 1994.
- [10] H. Nickel, "A detailed experimental study of the wet oxidation kinetics of $\text{Al}_x\text{Ga}_{1-x}\text{As}$ layers," *J. Appl. Phys.*, vol. 78, pp. 5201–5203, 1995.
- [11] F. A. Kish, S. J. Caracci, N. Holonyak, Jr., J. M. Dallesasse, K. C. Hsieh, M. J. Ries, S. C. Smith, and R. D. Burnham, "Planar native-oxide index-guided $\text{Al}_x\text{Ga}_{1-x}\text{As}$ -GaAs quantum well heterostructure lasers," *Appl. Phys. Lett.*, vol. 59, pp. 1755–1757, 1991.
- [12] S. J. Caracci, F. A. Kish, N. Holonyak, Jr., S. A. Maranowski, S. C. Smith, and R. D. Burnham, "High-performance planar native-oxide buried-mesa index-guided algaas-GaAs quantum well heterostructure lasers," *Appl. Phys. Lett.*, vol. 61, pp. 321–323, 1992.
- [13] F. A. Kish, S. J. Caracci, N. Holonyak, Jr., P. Gavrilovic, K. Meehan, and J. E. Williams, "Coupled-stripe in-phase operation of planar native-oxide index-guided $\text{Al}_y\text{Ga}_{1-y}\text{As}$ -GaAs- $\text{In}_x\text{Ga}_{1-x}\text{As}$ quantum well heterostructure laser arrays," *Appl. Phys. Lett.*, vol. 60, pp. 71–73, 1992.
- [14] F. A. Kish, S. J. Caracci, S. A. Maranowski, N. Holonyak, Jr., S. C. Smith, and R. D. Burnham, "Planar native-oxide $\text{Al}_x\text{Ga}_{1-x}\text{As}$ -GaAs quantum well heterostructure ring laser diodes," *Appl. Phys. Lett.*, vol. 60, pp. 1582–1584, 1992.
- [15] S. J. Caracci, M. R. Krames, N. Holonyak, Jr., C. M. Herzinger, A. C. Crook, T. A. DeTemple, and P.-A. Besse, "Native-oxide-defined low-loss $\text{Al}_x\text{Ga}_{1-x}\text{As}$ -GaAs planar waveguide bends," *Appl. Phys. Lett.*, vol. 63, pp. 2265–2267, 1993.
- [16] S. J. Caracci, M. R. Krames, M. J. Ries, and N. Holonyak, Jr., "Planar single-facet teardrop-shaped $\text{Al}_x\text{Ga}_{1-x}\text{As}$ -GaAs quantum well heterostructure laser," *Appl. Phys. Lett.*, vol. 63, pp. 1818–1820, 1993.
- [17] W. D. Laidig, N. Holonyak, M. D. Camras, K. Hess, J. J. Coleman, P. D. Dapkus, and J. Bardeen, "Disorder of an algaas super-lattice by impurity diffusion," *Appl. Phys. Lett.*, vol. 38, pp. 776–778, 1981.
- [18] M. R. Krames, E. I. Chen, and N. Holonyak, Jr., "Deep-oxide planar buried-heterostructure AlGaAs-GaAs quantum well heterostructure laser diodes," *Appl. Phys. Lett.*, vol. 65, pp. 3221–3223, 1994.
- [19] M. R. Krames, E. I. Chen, N. Holonyak, Jr., A. C. Crook, T. A. DeTemple, and P.-A. Besse, "Deep oxide planar buried-channel $\text{Al}_x\text{Ga}_{1-x}\text{As}$ -GaAs quantum well heterostructure waveguides with low bend loss," *Appl. Phys. Lett.*, vol. 66, pp. 1912–1914, 1995.
- [20] M. R. Krames, A. D. Minervini, and N. Holonyak, Jr., "Deep-oxide curved resonator for low-threshold AlGaAs-GaAs quantum well heterostructure ring lasers," *Appl. Phys. Lett.*, vol. 67, pp. 73–75, 1995.
- [21] D. C. Hall, H. Wu, L. Kou, Y. Luo, R. J. Epstein, O. Blum, and H. Hou, "Refractive index and hygroscopic stability of $\text{Al}_x\text{Ga}_{1-x}\text{As}$ native oxides," *Appl. Phys. Lett.*, vol. 75, pp. 1110–1112, 1999.
- [22] F. A. Kish, S. J. Caracci, N. Holonyak, Jr., J. M. Dallesasse, A. R. Sugg, R. M. Fletcher, C. P. Kuo, T. D. Osentowski, and M. G. Craford, "Planar native-oxide buried-mesa $\text{Al}_x\text{Ga}_{1-x}\text{As-In}_{0.5}(\text{Al}_y\text{Ga}_{1-y})_{0.5}\text{P-In}_{0.5}(\text{Al}_z\text{Ga}_{1-z})_{0.5}\text{P}$ visible spectrum-heterostructure laser diodes," *J. Appl. Phys.*, vol. 71, pp. 2521–2525, 1992.
- [23] D. Liang, J. Wang, and D. C. Hall, "Oxide-confined high index contrast ridge waveguide curved resonator laser diodes," in *Proc. LEOS 2005: IEEE Lasers and Electro-Optics Society 18th Annu. Meeting*, Sydney, Australia, 2005, pp. 943–944.
- [24] S. A. Maranowski, N. Holonyak, Jr., T. A. Richard, and F. A. Kish, "Photon-induced anisotropic oxidation along p-n junctions in $\text{Al}_x\text{Ga}_{1-x}\text{As}$ -GaAs quantum well heterostructures," *Appl. Phys. Lett.*, vol. 62, pp. 2087–2089, 1993.
- [25] Y. Luo, D. C. Hall, L. Kou, L. Steingart, J. H. Jackson, O. Blum, and H. Hou, "Oxidized $\text{Al}_x\text{Ga}_{1-x}\text{As}$ heterostructure planar waveguides," *Appl. Phys. Lett.*, vol. 75, pp. 3078–3080, 1999.
- [26] Y. Luo, D. C. Hall, O. Blum, R. M. Sieg, and A. A. Allerman, "Fully-oxidized AlGaAs heterostructures as broadband passive waveguides for photonic circuit integration," in *Proc. LEOS 2000: IEEE Lasers and Electro-Optics Society 13th Annu. Meeting*, vol. 2, Rio Grande, Puerto Rico, 2000, pp. 708–709.
- [27] Y. Luo, "Optical Properties of AlGaAs Native Oxides for Optoelectronics Applications," Ph.D. dissertation, Dept. Elect. Eng., Univ. Notre Dame, Notre Dame, 2001.
- [28] B. S. Ooi, K. McIlvaney, M. W. Street, A. S. Helmy, S. G. Ayling, A. C. Bryce, J. H. Marsh, and J. S. Roberts, "Selective quantum-well intermixing in GaAs-AlGaAs structures using impurity-free vacancy diffusion," *IEEE J. Quantum Electron.*, vol. 33, no. 10, pp. 1784–1793, Oct. 1997.
- [29] L. Kou, D. C. Hall, and H. Wu, "Room-temperature 1.5 μm photoluminescence of Er^{3+} -doped $\text{Al}_x\text{Ga}_{1-x}\text{As}$ native oxides," *Appl. Phys. Lett.*, vol. 72, pp. 3411–3413, 1998.
- [30] L. Kou, D. C. Hall, C. Strohhofer, A. Polman, T. Zhang, R. M. Kolbas, R. D. Heller, and R. D. Dupuis, "Er-doped AlGaAs native oxides: photoluminescence characterization and process optimization," *IEEE J. Sel. Topics Quantum Electron.*, vol. 8, no. 4, pp. 880–890, Jul./Aug. 2002.
- [31] C. I. H. Ashby, J. P. Sullivan, K. D. Choquette, K. M. Geib, and H. Q. Hou, "Wet oxidation of AlGaAs: The role of hydrogen," *J. Appl. Phys.*, vol. 82, pp. 3134–3136, 1997.
- [32] O. Kubaschewski, C. B. Alcock, and P. J. Spencer, *Materials Thermochimistry*. London, U.K.: Pergamon, 1993.
- [33] R. D. Twesten, D. M. Follstaedt, K. D. Choquette, and R. P. Schneider Jr., "Microstructure of laterally oxidized $\text{Al}_x\text{Ga}_{1-x}\text{As}$ layers in vertical-cavity lasers," *Appl. Phys. Lett.*, vol. 69, pp. 19–21, 1996.
- [34] R. D. Twesten, D. M. Follstaedt, and K. D. Choquette, "Microstructure and interface properties of laterally oxidized $\text{Al}_x\text{Ga}_{1-x}\text{As}$," in *Vertical-Cavity Surface Emitting Lasers, Proc. SPIE*, K. D. Choquette and D. G. Deppe, Eds., vol. 3003, 1997, pp. 55–61.
- [35] S.-K. Cheong, B. A. Bunker, T. Shibata, D. C. Hall, C. B. DeMelo, Y. Luo, G. L. Snider, G. Kramer, and N. El-Zein, "The residual arsenic site in oxidized $\text{Al}_x\text{Ga}_{1-x}\text{As}$ ($x = 0.96$)," *Appl. Phys. Lett.*, vol. 78, pp. 2458–2460, 2001.
- [36] C. I. H. Ashby, M. M. Bridges, A. A. Allerman, B. E. Hammons, and H. Q. Hou, "Origin of the time dependence of wet oxidation of AlGaAs," *Appl. Phys. Lett.*, vol. 75, pp. 73–75, 1999.

Yong Luo was born in Hunan, China. He received the B.S. degree in 1992 from Tsinghua University, Beijing, China, and the M.S. degree in 1995 from Academia Sinica, Beijing, China, both in physics. He received the M.S.E.E. and the Ph.D. degrees in electrical engineering from the University of Notre Dame, Notre Dame, IN, in 1999 and 2001, respectively.

In 2000, he joined Agilent Technologies, San Jose, CA, where he worked on power amplifier and fiber optical transceiver products for wireless communication and telecommunication applications. Currently, he is working for a small semiconductor company in Twinsburg, OH. His research interests include nanoelectronics, wireless communication and high-speed IC design.

Douglas C. Hall (S'86–M'91) received the B.S. degree (*summa cum laude*) in physics from Miami University, Oxford, OH, in 1985, and the M.S. and Ph.D. degrees in electrical engineering from the University of Illinois, Urbana-Champaign, in 1988 and 1991, respectively.

He is currently an Associate Professor with the Department of Electrical Engineering, University of Notre Dame, Notre Dame, IN. From 1991 to 1994, he was with the U.S. Naval Research Laboratory, Washington, DC, where he investigated high-power laser amplifiers and erbium-doped fiber sources for fiber optic gyroscopes. He has been with Notre Dame since 1994, and his present compound semiconductor materials and device research is focused on understanding and developing new applications of native oxides for optoelectronic, electronic, and integrated photonic devices.

Dr. Hall is a member of the IEEE Lasers and Electro-Optics Society, the American Physical Society, the Optical Society of America, and the American Society for Engineering Education. He has three times been the recipient of the Teacher of the Year Award from the Department of Electrical Engineering at the University of Notre Dame.